

Stress-induced hydrogen self-trapping in tungsten

R. D. Smirnov* and S. I. Krasheninnikov

*University of California San Diego, Department of Mechanical and Aerospace Engineering,
9500 Gilman Drive, La Jolla, CA 92093-0411, USA*

*Corresponding author e-mail: rsmirnov@ucsd.edu

Keywords: hydrogen, tungsten, retention, fusion devices, molecular dynamics

Abstract

The molecular dynamics simulations of trapping of hydrogen atoms in tungsten are presented. The simulations reveal formation of platelet-like structures of self-trapped hydrogen induced by stresses in tungsten, in particular, those produced by dislocations, at the interstitial hydrogen concentrations $\sim 0.3 - 1$ at.%. The spontaneous hydrogen platelet formation in absence of dislocations and external stresses has been also observed at the higher hydrogen concentrations ~ 10 at.%. It is shown that the platelets can retain substantial quantities of hydrogen, exceeding trapping capacity of other non-cavity defects in tungsten. The properties of the hydrogen platelets formed in tungsten under various conditions are assessed and a formation mechanism is proposed. A model of hydrogen retention by the dislocation-induced structures is also presented, which describes retained quantities and outgassing dynamics of hydrogen in plasma exposed tungsten samples.

I. Introduction

It has been broadly recognized that plasma-material interactions in tokamaks present a major challenge for achieving practical fusion energy production due to both the impact of plasma on plasma-facing components and the contamination of fusion plasma with eroded wall material, e.g. see [1-3] and the references therein. In particular, the interactions of fusion plasma, consisting primarily of hydrogen isotopes (deuterium and tritium) and helium, with walls in tokamaks lead to dynamic exchange of plasma hydrogen with wall components, which complicates plasma fueling control and can cause accumulation of radioactive tritium in the wall material. The latter is critical for continuous fusion operation, as the total tritium amount in a tokamak is strictly limited due to safety considerations [4,5]. Hence, a choice of plasma-facing materials is crucially important for sustained fusion device operation.

Tungsten has been selected as material of plasma-facing divertor components in ITER tokamak and is considered as primary candidate for wall material in future fusion reactors owing to its low sputtering yield by hydrogen plasma and high melting point. While hydrogen does not chemically

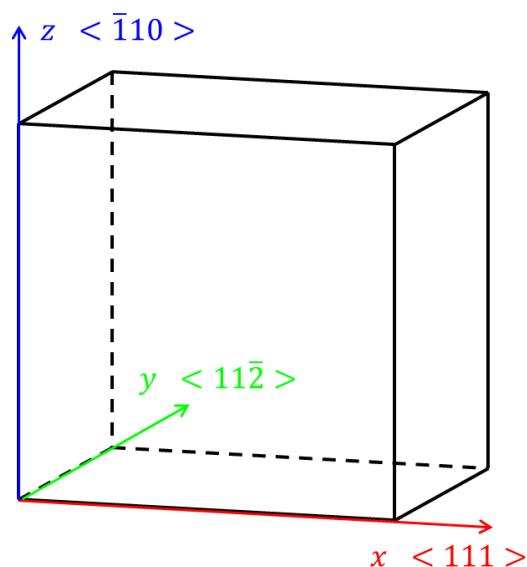
1
2
3 react with tungsten, concentrations of hydrogen as high as $\sim 0.1-1$ at.% are observed *post mortem*
4 in surface layers of thickness of several micrometers on tungsten samples exposed at temperatures
5 $< 600\text{K}$ to hydrogen plasma with ion fluxes and energies similar to those in divertor of current
6 tokamaks [6,7]. The programmed thermal desorption spectroscopy (TDS) analyses of the samples
7 show existence of various trapping sites for hydrogen in tungsten with de-trapping energies
8 ranging from ~ 0.7 eV to ~ 2.1 eV [8-11]. It is thought that hydrogen is primarily trapped by defects
9 in the material, such as vacancies and vacancy clusters, dislocations, and grain boundaries.
10 However, existing models of hydrogen transport and retention in tungsten, considering the
11 trapping by defects, do not satisfactorily explain some experimental observations. In particular,
12 available literature on density functional theory (DFT) modeling of hydrogen interactions with
13 defects in tungsten shows that only up to several hydrogen atoms can be trapped per a point defect
14 or a tungsten atom on dislocation line [12-15]. And, unlike helium, hydrogen does not produce
15 vacancy mutations and thus does not easily form bubbles in tungsten lattice. At the same time,
16 typical concentration of pre-existing point defects and fraction of tungsten atoms on dislocation
17 lines and grain boundaries in the tungsten samples are insufficient to account for the high density
18 of trapped hydrogen atoms observed in the experiments, in particular, ones using monocrystal
19 samples.
20

21
22 In this paper, we present first molecular dynamics (MD) simulations demonstrating hydrogen
23 self-trapping in interstitial positions in tungsten, either spontaneously at high interstitial hydrogen
24 concentrations $\gtrsim 10$ at.% or induced by dislocations and non-hydrostatic stresses at the lower
25 hydrogen concentrations $\lesssim 1$ at.%. We show that it leads to formation of extended dynamic
26 platelets of self-trapped hydrogen, which can contain thousands of hydrogen atoms per tungsten
27 atom on a dislocation line and close to 1:1 hydrogen-to-tungsten atomic ratio in the platelet
28 volume. We investigate the self-trapped hydrogen structure formation induced by edge and screw
29 dislocations at different temperatures and evaluate the hydrogen de-trapping energy from the
30 structures. A model describing amount of hydrogen trapped in the platelets is also presented, which
31 resolves the discrepancies of the previous hydrogen trapping models with experimental
32 observations.
33
34

35 36 37 38 39 40 41 42 **II. Simulation model**

43
44 We use LAMMPS molecular dynamics code [16] for the simulations reported in this paper.
45 The code is widely used for large variety of atomistic simulations including material studies for
46 fusion applications. The embedded atom method (EAM) empirical interatomic potential for
47 interactions between hydrogen and tungsten atoms, newly developed by Wang et al. [17], is
48 employed in the simulations. The potential has been fitted to extensive database of DFT
49 simulations with particular attention to accuracy of interactions of multiple hydrogen atoms with
50 clusters of point defects and of hydrogen transport in strained tungsten lattice. Such, the potential
51 successfully reproduces repulsion between interstitial hydrogen atoms in unstrained tungsten and
52 the dependencies of migration energy of a hydrogen atom between tetrahedral interstitial positions
53 on strain in hydrostatically, uniaxially, and biaxially strained bcc tungsten.
54
55
56
57
58
59
60

1
2
3 To investigate mechanisms of hydrogen trapping in tungsten, we generate bcc tungsten
4 monocrystal sample of size approximately 17x8x18 nm in x , y , and z directions, respectively,
5 which contains about 145 thousand tungsten atoms. The sample is orientated so that x axis
6 corresponds to its $\langle 111 \rangle$ crystallographic direction, y to $\langle 11\bar{2} \rangle$, and z to $\langle \bar{1}10 \rangle$, see figure 1.
7 The system is periodic in x and y directions, while the surface planes normal to z axis are free in
8 order to relax corresponding material stress components, as in surface layer of plasma exposed
9 tungsten. The lattice constant a is set initially equal to 3.162 Å that accommodates thermal
10 expansion of the lattice to produce near zero pressure in the system at temperatures ~ 1000 K. The
11 simulations proceeded with 1fs time step. Hydrogen atoms are inserted in the system every 10 ps
12 uniformly at random positions with subsequent minimization of their potential energy. As
13 hydrogen can leave the sample through the free surfaces, the number of inserted atoms varies such
14 that the total number of hydrogen atoms in the system is maintained constant at a given atomic
15 percentage relative to the tungsten atoms. The temperature of the system is kept constant using
16 Langevin thermostat for tungsten atoms and Berendsen velocity rescaling technique for hydrogen
17 with the same adjustment time scales of 0.1 ps. The Langevin thermostat for tungsten is selected
18 in order to dump any acoustic oscillations resulting from initial strains in the sample.
19
20
21
22
23
24
25



44 Figure 1. *Sketch of the simulated tungsten sample geometry. Color in this figure is available on-*
45 *line.*
46

47
48 Hydrogen dynamics is simulated in several sample configurations: perfect monocrystal
49 sample; sample containing various defects, i.e. edge dislocation, screw dislocation, vacancy; and
50 sample with various applied external stresses. Below we describe in detail each simulated
51 configuration and the corresponding simulation results. The majority of the simulations is
52 performed at the high system temperatures ~ 1000 K and the hydrogen densities from 0.3 to 10 at.%
53 in order to speed up kinetics of the processes in the sample due to very short computed time scale
54
55
56
57
58
59
60

~100ns achievable with MD method. The developed latter in this paper rate theory allows quantitative extrapolation of the simulations results to experiment relevant conditions.

III. Self-trapped hydrogen structures

a. Ideal crystal

First, we look into evolution of the initially perfect bcc tungsten lattice containing various quantities of interstitial hydrogen atoms at 1000 K. When the simulated average concentration of hydrogen was 0.3 and 1 at.%, no qualitative changes in tungsten lattice and hydrogen behavior were observed. The tungsten lattice remained unmodified, with no point defects or dislocations formed during the simulation time $t \sim 50$ ns. The hydrogen atoms occupied interstitial tetrahedral positions, forming no persistent clusters. As expected, hydrogen diffused toward the free surfaces establishing a non-uniform density profile along z axis, see figure 2. These simulations also confirm correctness of the used numerical method.

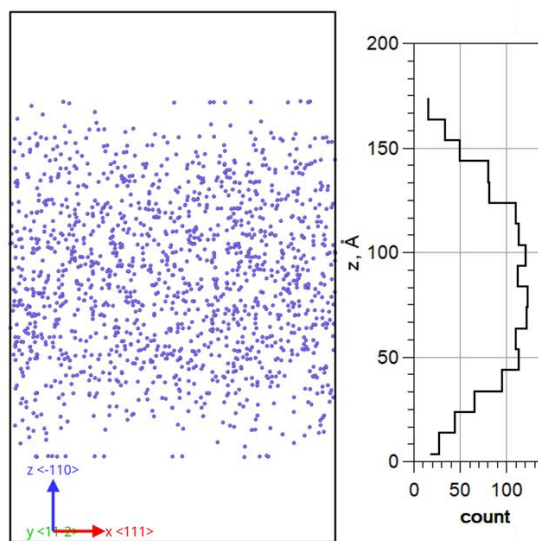
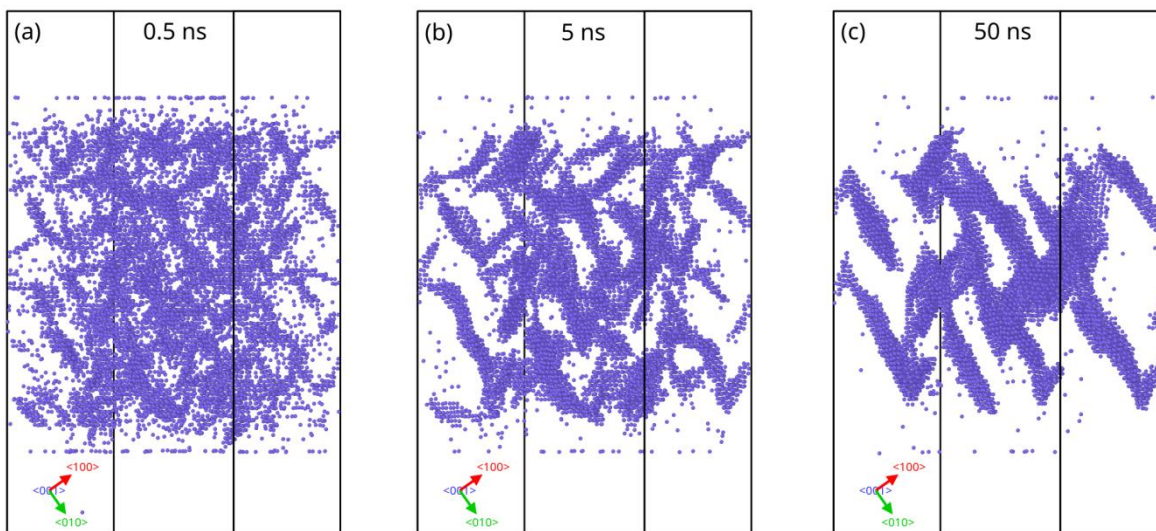


Figure 2. *Spatial distribution of hydrogen atoms (purple dots and right histogram) at 1 at.% average hydrogen density in the initially perfect bcc tungsten lattice at 46 ns simulated time. The black box on the left shows the simulation domain, where empty space is allowed above and below the sample's free surfaces. The vector tripod shows coordinate system used in the simulations. Color in this figure is available on-line.*

At the constant total hydrogen concentration of 10 at.%, however, the hydrogen behavior changed qualitatively. The hydrogen atoms quickly (on sub-nanosecond time scale) started to agglomerate into multiple platelets, see figure 3(a). We note that at 1 at.% hydrogen concentration, considered above, no hydrogen agglomeration occurred on ~ 100 times longer time scale, which

1
2
3
4 corresponds to the square of ratio of the simulated here hydrogen concentrations $(10 \text{ at.}\% / 1 \text{ at.}\%)^2$
5
6 . The tungsten lattice within the platelets is elastically strained due to hydrogen presence, where
7 the lattice stresses have predominantly bi-axial tension and shear character and are exceeding 10
8 GPa in magnitude. Common neighbor analysis of the tungsten atoms reveals that the lattice
9 transforms from bcc to fcc type within the volume of the hydrogen platelets. There are no tungsten
10 lattice point defects or dislocations produced and the hydrogen atoms occupy predominantly
11 octahedral interstitial positions within the platelets, unlike tetrahedral ones in the unmodified bcc
12 W lattice. The view shown in figures 3(a-c) highlights that the hydrogen platelets are preferentially
13 formed in certain planes, which can be approximately identified as [100], [110], and [120] type
14 planes of the initial bcc tungsten lattice.
15
16

17 At later simulated times, the number of hydrogen platelets decreases as they grow in size, see
18 figures 3(b,c). After several tens of nanoseconds, the platelets approach a steady-state
19 configuration with about 1:1 ratio of hydrogen-to-tungsten atoms and relatively low $\sim 0.1 \text{ at.}\%$, but
20 non-zero, concentration of “free” (not forming the platelets) hydrogen, which represents about 1%
21 of total hydrogen amount. This suggests that the hydrogen atoms are not permanently trapped
22 within the platelets and can detach from one and re-attach to another platelet, leading to a
23 dynamical equilibrium between trapped and free hydrogen. A direct evidence of hydrogen
24 dynamical behavior will be discussed in Section IV.
25
26
27
28



47
48
49
50
51
52
53
54
55
56
57
58
59
60

Figure 3. Platelet-like structures of self-trapped hydrogen atoms (purple dots) forming at 10 at.% hydrogen density in the initially perfect bcc tungsten lattice at 0.5 ns (a), 5 ns (b), and 50 ns (c) simulated time. The black lines represent edges of the simulation box. The vector tripod indicates principal directions of the initial bcc tungsten lattice. Color in this figure is available on-line.

1
2
3 The simulated behavior of hydrogen at the high concentrations in tungsten is indicative of
4 hydrogen self-trapping phenomenon, leading to formation of the platelets. It can be speculated that
5 chemical potential of interstitial hydrogen in tungsten depends on hydrogen density in non-
6 monotonic manner and has a local minima near or at 1:1 hydrogen-to-tungsten atomic ratio. Such
7 non-monotonic dependence of the chemical potential can be mediated by tungsten lattice
8 deformations, produced by the interstitial hydrogen itself, facilitating the hydrogen self-trapping
9 phenomenon. We note, that 1:1 stoichiometry also corresponds to the most stable form of tungsten
10 hydride, formation of which at high pressures was observed in DFT modeling [18] (although
11 having different hexagonal symmetry) and experimentally at 300K [19].
12
13
14
15
16

17 **b. Edge dislocation**

18
19 The high free hydrogen concentrations, $\gtrsim 10$ at.%, leading to the spontaneous formation of
20 the self-trapped hydrogen structures, as described in the previous section, in practice could be
21 achieved only in a very narrow (~ 10 nm) implantation layer near plasma irradiated tungsten surface
22 at low exposure temperatures and high plasma fluxes. However, hydrogen agglomeration into
23 extended self-trapping formations can be mediated by presence of dislocations even at the lower
24 concentrations. To investigate this possibility we created an edge dislocation line along y axis in
25 the center of (x,z) plane of the simulated tungsten sample with $\frac{1}{2}\langle 111 \rangle$ Burger's vector along x
26 direction. The dislocation has been prepared by inserting extra atomic half-layer and shifting the
27 tungsten atoms in accordance with elasticity theory using ATOMSK software [20]. The potential
28 energy of the tungsten system prepared in such way was subsequently minimized at the beginning
29 of the simulations.
30
31
32

33 In figure 4(a), the dislocation line and the hydrogen atoms in the tungsten sample containing 1
34 at.% of hydrogen at the temperature 1000 K are shown at 5 ns simulated time. One can see that
35 hydrogen started to aggregate along and below the dislocation line (in the tension region) forming
36 a symmetric platelet aligned with the dislocation slip plane (x,y) . Figure 4(b) shows the evolved
37 hydrogen platelet at 80 ns simulated time. At this stage the formed platelet-like structure is close
38 to a steady state and contains about 1300 or 90% of hydrogen atoms, corresponding to ~ 43
39 hydrogen atoms per tungsten atom on the dislocation line. As in the case without the dislocation,
40 the tungsten atoms rearrange into fcc lattice within the platelet, where hydrogen-to-tungsten atomic
41 ratio is close to 1:1 and a large part of the trapped hydrogen atoms occupy octahedral positions.
42 The concentration of "free" hydrogen is ~ 0.1 at.% at the steady state, indicating the same binding
43 energy of hydrogen to this platelet-like structure and the considered above spontaneously formed
44 platelets. These similarities point to self-trapping nature of the hydrogen agglomeration and
45 distinguish it from Cottrell atmospheres [21]. We also observe in figure 4(b) that the structure
46 growth crosses to $[021]$ plane, characteristic for the spontaneously formed platelets, creating the
47 asymmetric wing-like shape at the latter simulated stages. The structure's symmetry break can be
48 explained by increase of hydrogen binding energy to the structure with the distance from the
49 dislocation core. This contrasts with binding interstitial atoms by decaying with the distance
50
51
52
53
54
55
56
57
58
59
60

dislocation elastic stress field in Cottrell atmospheres. The dependence of the energy of hydrogen de-trapping from the platelet-like structure on its size is directly evaluated in Section IV.

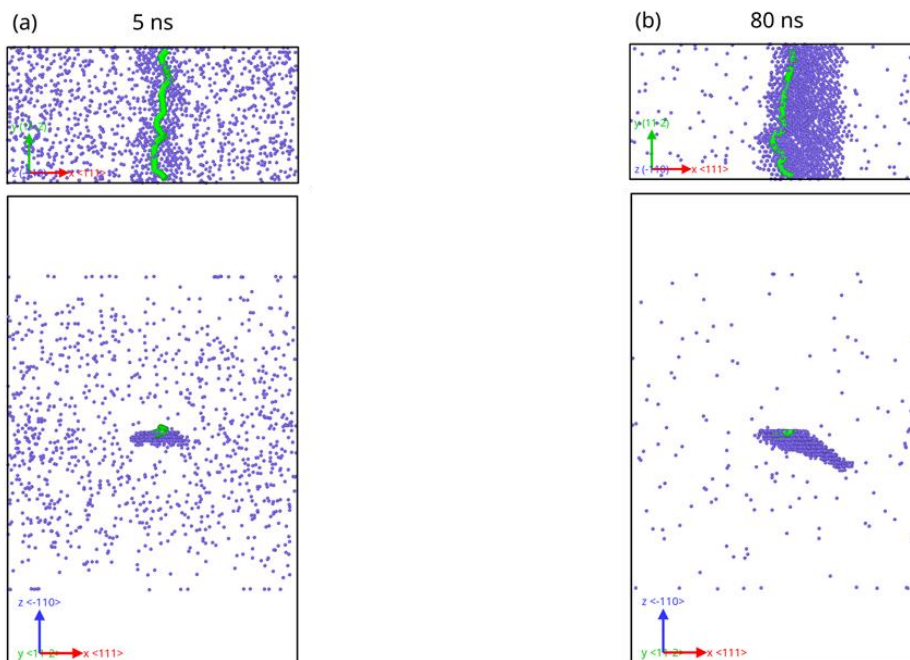


Figure 4. Top and front views of spatial distribution of hydrogen atoms (purple dots) near the edge dislocation (green line) in tungsten sample with 1 at.% hydrogen at 5 ns (a) and 80 ns (b) simulated time. The vector tripod shows coordinate system used in the simulations. Color in this figure is available on-line.

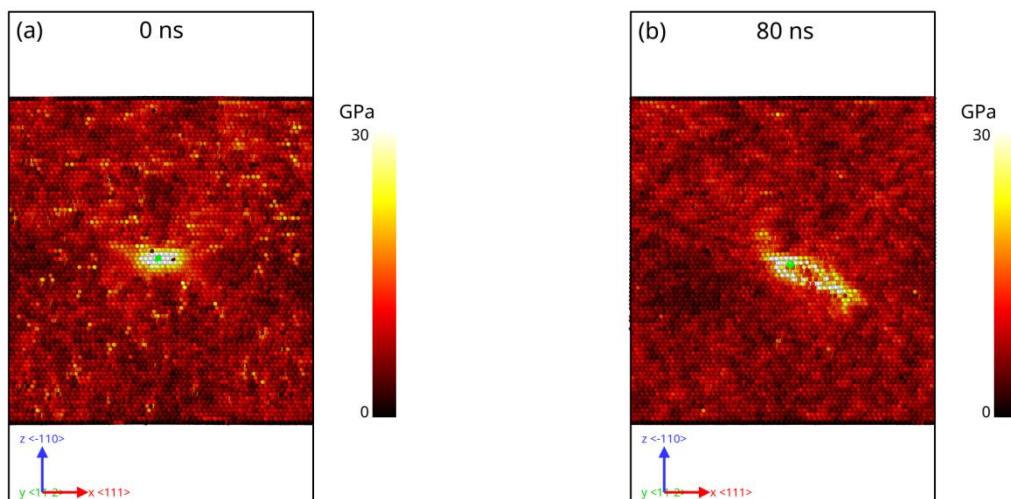
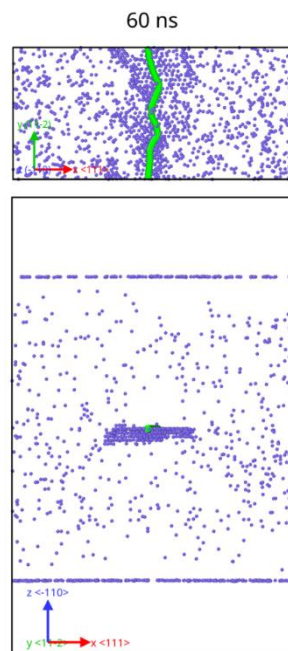


Figure 5. Profiles of von Mises stress in the tungsten sample containing edge dislocation at the start of the simulations (a) and 80 ns simulated time (b). The green dot in the sample center shows position of the dislocation line. Color in this figure is available on-line.

1
2
3 In figure 5, the profiles of von Mises stress on (x,z) plane drawn through the center of the
4 sample are plotted at the initial moment (a) and at 80 ns simulated time (b). The stress represents
5 magnitude of non-hydrostatic (deviatoric) stress tensor components and is used in the like named
6 plastic yield criterion. We use von Mises stress here, because hydrostatic stresses alone do not lead
7 to hydrogen agglomeration, as will be shown in Section III(d). Figure 5(a) demonstrates that the
8 initial region of large von Mises stress near the dislocation core has the shape elongated in x
9 direction similar to that of the trapped hydrogen platelet during the early formation stages. At the
10 later time, figure 5(b), the formed hydrogen structure leads to relaxation of the initial stresses in
11 vicinity of the dislocation line and creates its own stress field extending much farther from the
12 dislocation. We can see that the role of the dislocation is mostly limited to initiation of the
13 hydrogen agglomeration, while further growth of the platelet-like structure is supported by its own
14 stress field. We call this process induced hydrogen self-trapping.



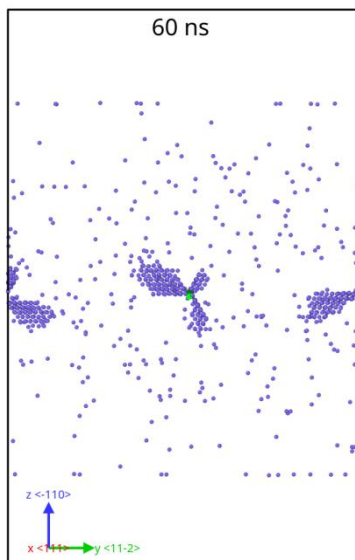
42 Figure 6. *Top and front views of spatial distribution of hydrogen atoms (purple dots) near the*
43 *edge dislocation (green line) in tungsten sample with 1 at.% hydrogen and 500 K*
44 *temperature at 60 ns simulated time. The vector tripod shows coordinate system used*
45 *in the simulations. Color in this figure is available on-line.*

46
47
48 In order to verify that formation of the hydrogen platelets is also possible at lower system
49 temperatures, we have simulated the same sample with edge dislocation as described above, but at
50 500 K temperature. In figure 6, the simulated distribution of hydrogen atoms near the dislocation
51 for the lower system temperature is shown at 60 ns simulated time. As one can see, the platelet
52 structure near the dislocation line is also formed in this case. However, as the hydrogen transport
53 is much slower at 500 K then at 1000 K, the simulated platelet is not yet fully developed during
54
55
56
57
58
59
60

1
2
3 the simulation. The general properties of the simulated hydrogen platelet at 500 K are the same as
4 those at 1000 K. This confirms that the qualitative platelet formation mechanism is at play even
5 for the lower temperatures albeit at slower rate. Thus, the rate theory developed further in the paper
6 can be reasonably applied to describe platelet formation dynamics in a range of the system
7 temperatures.
8
9

10 11 12 **c. Screw dislocation**

13 We also study hydrogen behavior in presence of a screw dislocation. We use here a tungsten
14 sample of approximate size $8 \times 17 \times 18$ nm in x , y , and z dimensions, respectively. A screw
15 dislocation line with $\frac{1}{2}\langle 111 \rangle$ Burger's vector, where both the line and the vector lay along x axis,
16 was created in the center of (y,z) plane of the sample using ATOMSK software. Total hydrogen
17 amount corresponding to 1 at.% average density and the system temperature of 1000 K were
18 maintained as described in Section II.
19
20
21
22



41
42
43
44
45
46
47
48
49
50
51
52
53
54
55
56
57
58
59
60

Figure 7. *Self-trapped hydrogen structures (purple dots represent hydrogen atoms) around the screw dislocations (green dots) in tungsten sample with 1 at.% of hydrogen at 60 ns simulated time. The vector tripod shows coordinate system used in the simulations. Color in this figure is available on-line.*

In figure 7, the spatial distribution of hydrogen atoms in the sample is shown at 60 ns simulated time. A mirror screw dislocation with opposite Burger's vector at the edge of the sample formed due to the periodic boundary conditions used in y direction. One can see in figure 7 that the screw dislocations have induced formation of self-trapped hydrogen structures around them. However, the structures have a three blade propeller shape unlike the wing shape in the case of edge dislocation. The hydrogen aggregation starts on $[112]$ type slip planes of the screw dislocations and then crosses into $[110]$ and $[120]$ type planes characteristic of the spontaneously formed

hydrogen platelets. This produced a spiral character of the platelet structure along the dislocation line that had a discontinuity at one location, where the platelets formed at different planes. We can also see that the blade platelets of the structures are unevenly developed, supporting the notion of larger binding energy of hydrogen atoms to the structure farther away from the dislocation line. As in the previous cases, tungsten atoms form fcc lattice within portion of the hydrogen platelets, where they cross into [110] and [120] type planes. Close to the dislocation core, tungsten lattice structure is distorted and cannot be easily identified and so are the hydrogen interstitial positions in this region. The hydrogen-to-tungsten atomic ratio within the structures is approaching 1:1 and the free hydrogen concentration is ~ 0.1 at.% similar to the considered above cases.

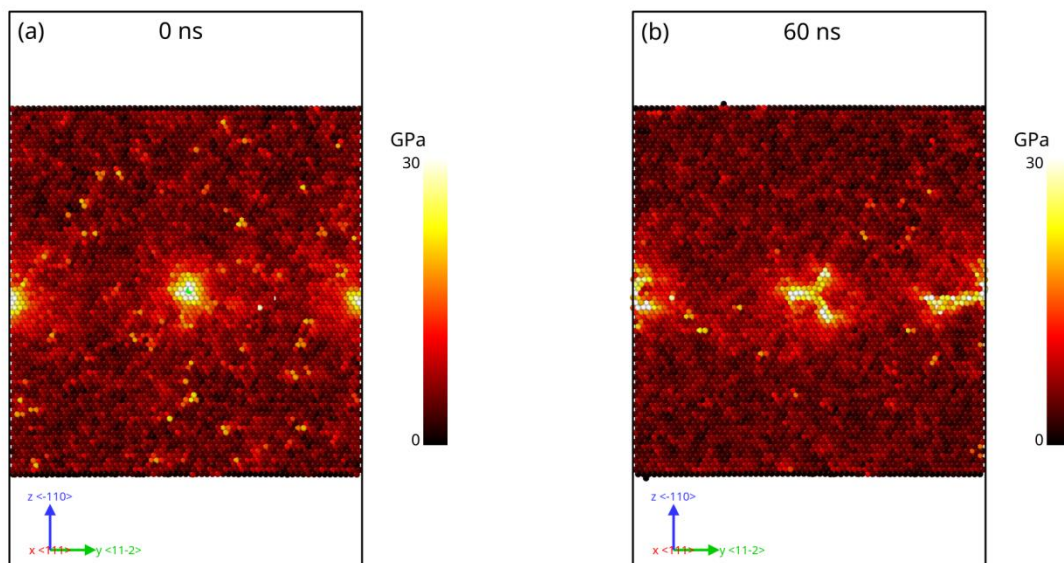


Figure 8. Profiles of von Mises stress in the tungsten sample containing screw dislocations at the start of the simulations (a) and 60 ns simulated time (b). The green dots in the sample center represent positions of the dislocation lines. Color in this figure is available on-line.

Figure 8 shows profiles of von Mises stress in the (y,z) plane drawn through the center of the system with the screw dislocations at the start of the simulation and at 60 ns simulated time. In figure 8(a) we can see that the initial stress field is concentrated close to the screw dislocations and has more triangular symmetry that defines shape of the hydrogen structure at initial formation stages. At the later time, figure 8(b), the stresses distinctly follow the shape of the structure and have little resemblance to the initial stress profile. We also should note here that screw dislocations do not produce hydrostatic stresses in the lattice. It follows that interaction of interstitial hydrogen atoms with deviatoric stress components of the dislocations initiate hydrogen platelet formation, which further generates its own stresses supporting growth of the structures. Thus, despite the difference in appearance of the hydrogen structures around screw dislocations, they have the same induced self-trapping formation mechanism as near edge dislocations.

d. Applied external stresses

As shown above, the stresses generated by dislocations play essential role in initiation of the hydrogen agglomeration. To directly observe effect of various stress components, we simulated evolution of hydrogen in tungsten samples with externally applied stresses.

Firstly, we applied periodic boundary conditions along all three axes and uniformly compressed or stretched the ideal bcc tungsten lattice by changing the lattice constant to 3.085 Å and 3.241 Å, respectively. That created homogeneous negative or positive strain of ~2.5% and corresponding pressure ~12GPa in the system. In these cases no formation of the hydrogen platelets was observed at 1 at.% hydrogen concentration, which affirms that hydrostatic stress alone neither compressive nor tensile does not induce hydrogen agglomeration.

Next, we removed the periodic boundary condition along z axis, allowing the tungsten sample to relax stress components in this direction, while applying the negative or positive strain in x and y directions as described above, which effectively produced biaxial stress in (x,y) plane in the system. In this case, the spontaneous formation of hydrogen platelets at 1 at.% concentration was observed only under tensile conditions, see figure 9(a). At the simulated time of 46 ns, shown in figure 9(a), we observe the free hydrogen concentration ~0.4 at.% that is higher than in the other considered cases, which can be due to non-steady-state stage of the platelet formation at the given moment related to slower initiation of the hydrogen agglomeration by external stresses, as described below.

Similarly, the hydrogen self-trapping was observed when a pure shear stress ~6 GPa was produced in (x,y) planes along x axis in the sample with 1 at.% of hydrogen by applying antiparallel forces to the sample's top and bottom free surfaces, figure 9(b). The self-trapped hydrogen structures formed with the applied external stresses have the same basic properties, as described in the previous sections. It appears, however, that the time needed to initiate formation of the hydrogen platelets depends on the applied stress magnitude. At the applied ~6GPa external shear stress the platelets did not form until ~50 ns into the simulations. When the shear stress of ~12GPa was applied, the formation of platelets happened about twice sooner. However, with ~12 GPa applied shear stress the tungsten sample yielded at approximately 30 ns simulated time and plastic flow initiated accompanied with spontaneous generation of dislocations. This suggests that presence of the self-trapped hydrogen structures can lower tungsten yield strength, similar to dissolved helium [22]. We also note that no tungsten lattice defects formed due to hydrogen presence before the yield occurred.

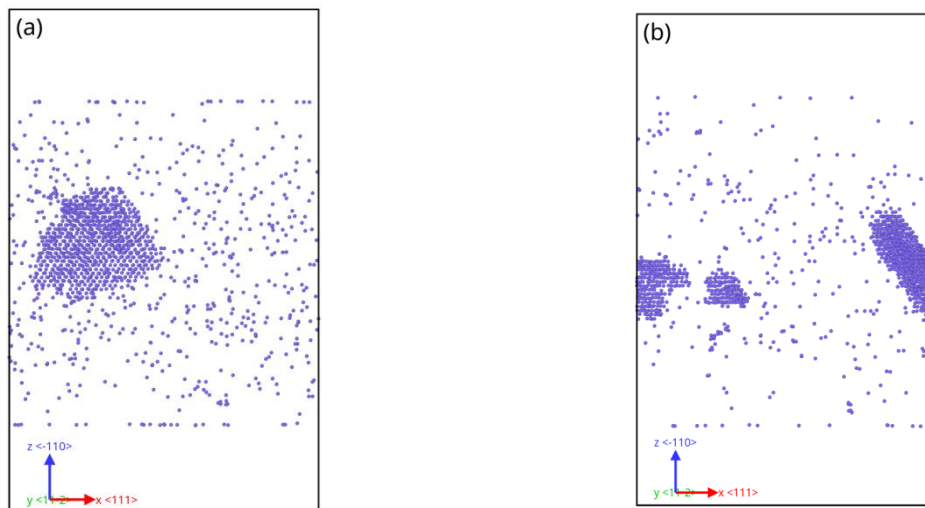


Figure 9. Platelets of self-trapped hydrogen atoms (purple dots) formed at 1 at.% hydrogen concentration in tungsten sample with applied bi-axial tensile stress at 46 ns simulated time (a) and with pure shear stress ~ 6 GPa at 100 ns (b). Color in this figure is available on-line.

The simulated behavior of hydrogen in the tungsten samples under the external stresses demonstrate that hydrogen atoms tend to agglomerate when sufficiently large non-hydrostatic stress components are present. This is likely associated with the nature of the lattice stresses produced by hydrogen atoms in tetrahedral interstitial positions, which are asymmetric relative to bcc tungsten atoms. That is consistent with absence of hydrogen platelet formation, when 1 at.% of hydrogen atoms were simulated in tungsten lattice in presence of a vacancy. In such case, up to 5 hydrogen atoms were trapped in the vacancy at any given simulation moment, however, this did not induce further hydrogen agglomeration and the platelet formation. An important role of anisotropic lattice stresses is also supported by simulated changes of hydrogen solution energy and tendency of interstitial hydrogen atoms to shift from tetrahedral to octahedral positions in tungsten when anisotropic strain is applied [23].

The obtained results allow us to speculate that the interaction of interstitial hydrogen with the non-hydrostatic stress components initially reduces the tungsten lattice elastic field energy enabling the hydrogen atoms to overcome mutual repulsion in the tungsten lattice. This leads to clustering of hydrogen atoms and local transformation of tungsten lattice from bcc to fcc type, which further induces stresses in bcc tungsten and hydrogen agglomeration. Such mechanism could be verified experimentally comparing trapped hydrogen amounts in unstressed and bi-axially stretched or sheared tungsten samples.

IV. Formation dynamics

In figure 10, the side view of the hydrogen platelet-like structure formed near the edge dislocation is shown at 80 ns and 90 ns simulated times close to steady-state. The hydrogen atoms forming the platelet at 80 ns time moment are highlighted in red. We can see in the figure that at 90 ns some of the highlighted hydrogen atoms have left the platelet and other hydrogen atoms from the surrounding volume have replaced them. This illustrates that the formation and subsistence of the self-trapped hydrogen structures is an essentially dynamical process. The dynamical nature of the structures can provide an alternative explanation for hydrogen isotope exchange at lower temperatures proposed for tritium extraction, without need for multi-occupancy stage causing decrease of de-trapping energy from other hydrogen trapping sites, such as vacancies [24].

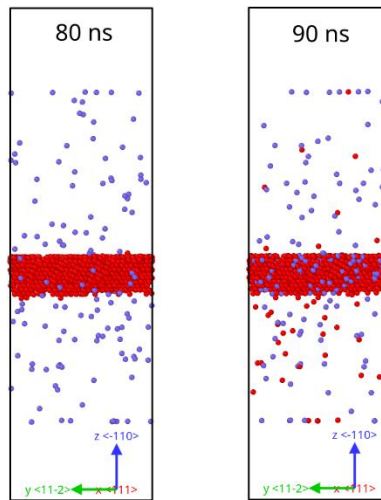


Figure 10. *Spatial distributions of atoms belonged (red) and not belonged (purple) to the hydrogen platelet-like structure at 80 ns and their dynamical re-distribution at 90 ns simulated time. Some of the free hydrogen atoms are projected over the platelet. Color in this figure is available on-line.*

The temporal evolution of the number of hydrogen atoms, $N_H(t)$, forming the platelet near the edge dislocation at the different total hydrogen concentrations and the system temperatures, T , is plotted in figure 11. We can see in figure 11(a) that the number of hydrogen atoms in the platelet gradually increases from zero approaching a steady-state value. The steady-state level rises with increasing hydrogen concentration in the system; however, it is not exactly proportional to the concentration. This can be attributed to the dependence of the hydrogen de-trapping energy on the size of the platelet, as will be shown below. The steady-state size of the platelet also depends on the system temperature, figure 11(b). The size decreases with the temperature, showing that the rate of hydrogen de-trapping from the platelet increases with the temperature faster than the

trapping rate. We can also see that the imposed increase of the system temperature from 1000 K to 1300 K and 1500K at ~ 91 ns, when the structure has already developed, leads to the reduction of the number of trapped hydrogen atoms (the plotted decaying branches) to the steady-state levels corresponding to structure growth (the plotted increasing branches) at the respective temperatures. Therefore, the formation dynamics does not exhibit hysteresis effects and the steady-state platelet size can be described based on current system temperature and hydrogen concentration.

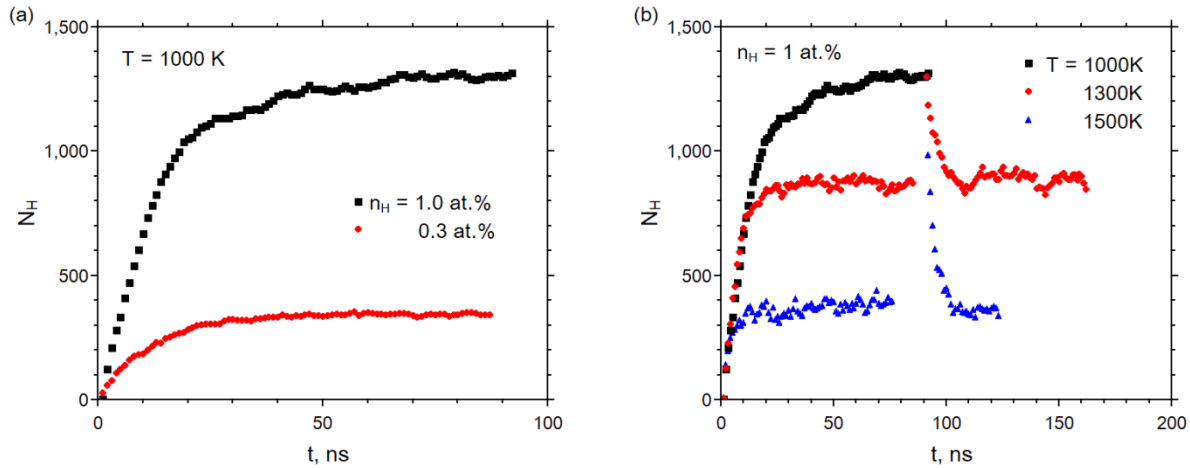


Figure 11. *Temporal evolution of number of hydrogen atoms forming the platelet-like structure near the edge dislocation at the different total hydrogen concentrations for 1000 K system temperature (a) and at 1 at.% total hydrogen concentration for the different system temperatures (b). The increasing dependencies correspond to the platelet formation from the initially random hydrogen spatial distribution. The decaying dependencies correspond to evolution of the previously formed platelet at the increased system temperatures. Color in this figure is available on-line.*

In order to evaluate the de-trapping energy of hydrogen atoms from the platelet, E_{dt} , we counted the number of hydrogen atoms, $N_{dt}(t, \Delta t)$, leaving the platelet formed near the edge dislocation at time t during time interval $\Delta t = 1$ ns. This number can be estimated as

$$N_{dt}(t, \Delta t) = N_H(t) \nu_{H0} \Delta t \exp\left(-\frac{E_{dt}}{k_B T}\right), \quad (1)$$

where $\nu_{H0} \approx 5.2 \times 10^{11} \text{ s}^{-1}$ is the hydrogen atom transition attempt frequency. This frequency is evaluated by dividing by a^2 the pre-exponential factor of the hydrogen diffusion coefficient $D_H = 5.3 \cdot 10^{-8} [\text{m}^2 \text{ s}^{-1}] \exp(-0.23 [\text{eV}] / k_B T)$, which was fitted to the employed EAM interatomic potential [17]. Using expression (1) and knowing the number of hydrogen atoms forming the platelet, $N_H(t)$, as function of time with 1 ns step, we can obtain the de-trapping energy as

function of N_H , which is plotted in figure 12 for the different system temperatures. The data points plotted in this figure are clustered near the steady-state N_H values and exhibit significant noise. Nevertheless, the plot shows that the de-trapping energy generally increases with N_H , confirming such notions in the previous sections. Moreover, the significant difference in the values of E_{dt} at 1000 K and the higher temperatures indicates dependence of the de-trapping energy on the system temperature, which can be due to effect of thermal expansion of the tungsten lattice. Using the plotted data, the values of E_{dt} corresponding to the steady-state platelet sizes can be evaluated as 0.871 ± 0.038 eV at 1000 K, 0.947 ± 0.025 eV at 1300 K, and 0.929 ± 0.026 eV at 1500 K, where the errors have 95% confidence interval. We should note, that using an alternative value of $\nu_{H0} \approx 10^{13} \text{ s}^{-1}$, as in many published TDS analyses, would produce higher E_{dt} values of 1.126 ± 0.038 eV, 1.278 ± 0.025 eV, and 1.311 ± 0.026 eV at 1000 K, 1300 K, and 1500 K, respectively. All the obtained E_{dt} values are in the range of hydrogen de-trapping energies derived from TDS experiments on tungsten samples exposed to hydrogen plasmas [8-11]. Below we use only the de-trapping energies consistent with the atomic potential employed in the simulations. The obtained here variations of the hydrogen de-trapping energy on the platelet size and the system temperature can also explain the observed widening of TDS peaks, otherwise requiring an assumption of existence of multiple kinds of hydrogen traps in tungsten with close de-trapping energies [25].

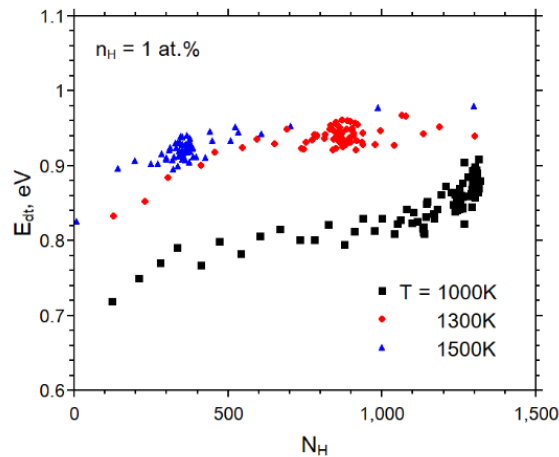


Figure 12. *The evaluated hydrogen atom de-trapping energy from the platelet-like structure formed near the edge-dislocation as function of the number of hydrogen atoms in the structure for the different system temperatures. Color in this figure is available on-line.*

V. Hydrogen retention in the structures

Here we consider a simple model of hydrogen trapping on a dislocation-induced structure assuming that the linear size of the platelet-like structure along the dislocation line is much larger than its transversal size and that the flux of free hydrogen atoms to the structure is diffusion limited. The first assumption is usually satisfied as most stable dislocations existing in metals tend to have length much exceeding the modelled here transversal platelet sizes of a few nanometers. The second assumption is valid when the diffusion dominates hydrogen transport in the collection basin of the platelet. This assumption can require further detailed investigation of stresses generated by the platelets. However, as the diffusion of hydrogen atoms in tungsten is sufficiently fast the size of the collection basin is likely to exceed the spatial extend of the stress field, which quickly decays with the distance from the platelets, see figures 5 and 8. Under these assumptions, we can neglect details of the structure shape and describe its characteristic transversal size with a parameter R_s using one-dimensional radial approximation. Then, introducing the linear density of trapped hydrogen atoms, $\eta = N_H / L$, where L is the dislocation length, we can describe the collection of hydrogen by the structure as

$$\left(\frac{\partial \eta}{\partial t} \right)_{collect} = 2\pi r D_H \frac{\partial n_H}{\partial r}, \quad (2)$$

where r is the radial coordinate perpendicular to the dislocation line, and n_H is the density of free hydrogen in tungsten lattice. Integrating equation (2) from R_s to a characteristic radius of the collection basin R_c we obtain

$$\left(\frac{\partial \eta}{\partial t} \right)_{collect} = \frac{2\pi D_H n_{H0}}{\ln(R_c/R_s)}, \quad (3)$$

where n_{H0} is the free hydrogen density at the far end of the collection basin.

The de-trapping of hydrogen from the structure is described by equation (1), which can be rewritten as follows

$$\left(\frac{\partial \eta}{\partial t} \right)_{de-trap} = -\eta v_{dt}, \quad (4)$$

where $v_{dt} = v_{H0} \exp(-E_{dt}/k_B T)$. In the steady-state the number of collected and de-trapped hydrogen atoms per unit length of the structure balance each other, in which case from equations (3) and (4) we get

$$\eta_{eq} = \frac{2\pi D_H n_{H0}}{v_{dt} \ln(R_c/R_s)}. \quad (5)$$

1
2
3 The logarithm in the denominator of equation (5) is a weak function of the structure's and the
4 collection basin's sizes when $R_c/R_s \gg 1$. For practical purposes we can often neglect this
5 dependence and treat the parameter $\Lambda \equiv \ln(R_c/R_s)$ approximately as a constant. The characteristic
6 size of the collection basin can be estimated as the average distance between dislocation lines,
7 $R_c \sim \rho^{-1/2}$, where ρ is the dislocation density. In the simulated periodic system with one
8 dislocation line crossing the surface of approximately $17 \times 18 \text{ nm}^2$ the dislocation density is
9 $\rho \sim 3 \cdot 10^{15} \text{ m}^{-2}$, then for $R_s \sim 3 \text{ nm}$ we have $\Lambda \sim 2$. Using the following values of the parameters,
10 $E_{dt} \sim 0.9 \text{ eV}$, $n_{H0} \sim 10^{26} \text{ m}^{-3}$, $v_{dt} \sim 10^7 \text{ s}^{-1}$, and $D_H \sim 4 \cdot 10^{-9} \text{ m}^2 \text{ s}^{-1}$, corresponding to our
11 simulations at $T \sim 1000 \text{ K}$, we obtain from equation (5) $\eta_{eq} \sim 10^{11} \text{ atoms/m}$, which is of the same
12 order of magnitude as the simulation results (~ 1000 atoms per $\sim 10 \text{ nm}$ of dislocation length). Thus,
13 the model equation (5) gives a reasonable estimate of steady-state amount of hydrogen contained
14 in the self-trapped structures induced by dislocations.
15

16
17 For the dislocation density $\rho \sim 10^{13} \text{ m}^{-2}$ that was measured in ITER specification tungsten
18 samples exposed to hydrogen plasma [26], we have $\Lambda \sim 5$. Then for typical temperature of the
19 samples during plasma exposure $T \sim 500 \text{ K}$ using formula (5) we obtain $\eta_{eq} \rho \sim 10 n_{H0}$, so that the
20 amount of hydrogen trapped in the dislocation-induced structures is about an order of magnitude
21 larger than of the free hydrogen. With decreasing temperature the part of the trapped hydrogen
22 rapidly increases and can exceed that of the free hydrogen by several orders of magnitude. Such,
23 at the room temperature $T \sim 300 \text{ K}$ practically all hydrogen would be trapped in the platelets
24 $\eta_{eq} \rho \sim 10^5 n_{H0}$. For $\rho \sim 10^{13} \text{ m}^{-2}$ and the total hydrogen concentration $\sim 0.1 \text{ at.}\%$, such η_{eq} would
25 correspond to the number of trapped hydrogen atoms $\sim 10^3$ per one tungsten atom on a dislocation
26 line, much exceeding trapping capacity of other non-cavity defects. Moreover, as we saw in the
27 simulations, presence of the hydrogen platelets can facilitate generation of new dislocations under
28 stresses, which can be produced in the material surface layer due to plasma heat and particles
29 fluxes. Such, the measured dislocation density in the hydrogen implantation region (first several
30 nanometers below the tungsten sample surface) was $\sim 10^{15} \text{ m}^{-2}$ [26]. This can lead to the much
31 higher density of the trapped hydrogen close the plasma exposed surface in agreement with
32 experimental observations [6,7,26,27]. In addition, in fusion reactors neutron irradiation can also
33 cause generation of dislocations and other defects through the material volume [28-30], which
34 would facilitate hydrogen trapping in the wall bulk.
35

36 To estimate life-time of the hydrogen platelets under outgassing conditions, we need to
37 consider dynamics of hydrogen in a tungsten sample. Assuming that surface recombination of
38 hydrogen does not limit its outgassing and considering a hydrogen retaining layer of characteristic
39 width Δx beneath the sample surface, we can write the following 0-dimensional hydrogen
40 dynamics equations for the layer
41
42
43
44
45
46
47
48
49
50
51
52
53
54
55
56
57
58
59
60

$$\frac{\partial \eta}{\partial t} = \frac{2\pi D_H}{\Lambda} n_{H0} - \nu_{dt} \eta, \quad (6)$$

$$\frac{\partial n_{H0}}{\partial t} = -\frac{D_H}{\Delta x^2} n_{H0} - \rho \frac{\partial \eta}{\partial t}. \quad (7)$$

Looking for solutions of these equations in the form $\eta, n_{H0} \sim \exp(-t/\tau)$, where τ is the characteristic time of hydrogen retention in the layer, we find the decaying in time solutions with

$$\tau \approx \frac{2\pi\rho\Delta x^2}{\Lambda\nu_{dt}}, \quad (8)$$

when condition $\nu_{tr} \equiv 2\pi D_H \rho / \Lambda \gg D_H / \Delta x^2, \nu_{dt}$ is satisfied. Here ν_{tr} is the frequency of trapping of the free hydrogen atoms by the platelets. Using values $\nu_{dt} \sim 4 \cdot 10^{-4} \text{ s}^{-1}$ and $D_H \sim 7 \cdot 10^{-12} \text{ m}^2 \text{ s}^{-1}$, corresponding to sample storage conditions at the room temperature, $\rho \sim 10^{13} \text{ m}^{-2}$ and Δx from $\sim 1 \text{ }\mu\text{m}$ to $\sim 10 \text{ }\mu\text{m}$ (which correspond to the experimental findings [26] and satisfy the above condition) from equation (8) we obtain $\tau \sim 10^5 - 10^7 \text{ s}$. Thus, the amount of hydrogen trapped in the dislocation-induced structures in such sample would gradually decay on the time scale of order of days to several months. This is consistent with the experimental studies of storage time effects on hydrogen retention in the plasma exposed tungsten samples [31,32].

We should note that the characteristic retention time τ is much longer than ν_{dt}^{-1} because of the slow effective diffusion of hydrogen in the layer governed by continuous re-trapping of free hydrogen by the platelets. The effective hydrogen diffusion coefficient can be written as $D_{H,eff} = D_H \nu_{dt} / \nu_{tr}$ and because the trapping frequency itself is proportional to D_H , the retention time τ does not depend on the diffusion coefficient. However, at the elevated temperatures $T \sim 600 \text{ K}$, ν_{tr} and ν_{dt} are of the same order of magnitude, so the hydrogen diffusion is not effectively slowed by the platelets. This could allow hydrogen to propagate deep into the samples even as the platelets are formed. Consideration of neglected here hydrogen surface recombination effects may further increase the retention time.

VI. Conclusions

The molecular dynamics simulations performed in this work demonstrate possibility of formation of self-trapped hydrogen atomic structures in tungsten induced by dislocations and external non-hydrostatic stresses at the interstitial hydrogen concentrations of order of 0.3 – 1 at.%. The formed hydrogen structures have platelet-like geometry and lay preferentially in [100], [110], and [120] type planes of tungsten lattice. The common neighbor analysis of tungsten atoms reveals that tungsten lattice changes from bcc to fcc type within the platelets. No crystal defects are produced in the platelets, where significant part of the trapped hydrogen atoms occupies octahedral interstitial positions, as compared to usual tetrahedral interstitial hydrogen positions in bcc tungsten. The hydrogen-to-tungsten atomic ratio within the platelets is close to 1:1, which

1
2
3 corresponds to the stoichiometry of the most stable form of tungsten hydride. The structures
4 formed on dislocations have transversal size of order of several nanometers and can contain
5 thousands of hydrogen atoms per one tungsten atom on a dislocation line that differs them
6 significantly from other non-cavity kind of traps of hydrogen in tungsten. We should note here that
7 hydrogen decorated screw dislocations in plasma exposed tungsten had been experimentally
8 observed [12]. The performed simulations also demonstrated spontaneous formation of the
9 hydrogen platelets in tungsten sample without initial stresses at the higher hydrogen concentrations
10 ~ 10 at.%.
11

12
13
14 Analysis of von Mises stresses in the tungsten lattice during the platelet formation indicate that
15 the mechanism of the hydrogen agglomeration is related to interaction of interstitial hydrogen
16 atoms with tungsten lattice non-hydrostatic tensile and shear stress components, which allows
17 overcoming repulsion of hydrogen atoms in the lattice and forming of hydrogen clusters. The
18 hydrogen clusters induce local transformation of tungsten lattice from bcc to fcc and generate
19 stresses, which cause further growth of the platelets by hydrogen self-trapping. Thus, the platelet
20 formation is in essence a collective phenomenon, which can be formally described with a non-
21 monotonic dependence of interstitial hydrogen chemical potential on hydrogen density in tungsten,
22 having a local minimum near 1:1 hydrogen-to-tungsten atomic ratio. The observed properties of
23 the self-trapped hydrogen structures and the proposed mechanism of their formation are essentially
24 different from those of Cottrell atmospheres near dislocations in metals.
25

26
27
28 The performed simulation of the system with the edge dislocation and 1 at.% hydrogen at 500
29 K also demonstrated formation of the hydrogen platelets near the dislocation line. This confirms
30 that the platelet formation mechanism persists and that a rate theory describing the formation
31 dynamics can be reasonably applied in a range of system temperatures. In addition, it is possible
32 that formation of the platelets on dislocation lines may proceed even at lower than simulated here
33 concentrations of free hydrogen, as the dislocation stress field facilitating start of hydrogen
34 agglomerations is initially always present and our simulations showed that structures continue to
35 slowly grow toward a saturation level even with remaining free hydrogen concentration ~ 0.1 at.%.
36

37
38
39 The de-trapping energy of hydrogen atoms from the platelet-like structures is evaluated using
40 de-trapped atoms statistics. The energy is found to have tendency to increase when the size of the
41 platelets or the temperature increase. In a steady-state at the high temperatures ~ 1000 K the de-
42 trapping energy was found to be around ~ 0.9 eV, which is in the range of the de-trapping energies
43 of hydrogen in plasma exposed tungsten samples experimentally measured using TDS techniques.
44 The variations of the de-trapping energy on platelet size and temperature can also explain
45 experimentally observed widening of the TDS peaks. Such de-trapping energies cause the platelets
46 to be very dynamic at the elevated temperatures, where hydrogen atoms are continuously trapped
47 and de-trapped from the platelets. The dynamic properties of the hydrogen platelets naturally
48 facilitate isotope exchange process for tritium extraction at lower wall temperatures, which
49 otherwise relies on multi-occupancy effects for traps with larger de-trapping energies, such as
50 vacancies.
51
52
53
54
55
56
57
58
59
60

1
2
3 The simulated with MD method high hydrogen concentrations could potentially be achieved
4 only at low wall temperatures and very high plasma fluxes. However, the developed simple
5 hydrogen retention model allows theoretical extrapolation of the simulated results and evaluation
6 of amount of hydrogen trapped in tungsten by the dislocation-induced structures under experiment
7 relevant steady-state conditions. The model shows that for the typical sample temperatures ~500
8 K during plasma exposure experiments and the measured dislocation densities in ITER grade
9 tungsten the volume averaged density of hydrogen retained by the platelet-like structures is by an
10 order of magnitude larger than that of the free hydrogen. At lower temperatures the retained
11 hydrogen density can exceed the free hydrogen density by many orders of magnitude. Thus, the
12 self-trapped hydrogen structures can accommodate amount of retained hydrogen corresponding to
13 the high ~0.1 at.% average density measured in plasma exposed tungsten samples. Moreover, it is
14 found that presence of the hydrogen platelets facilitates generation of dislocations under stress
15 conditions, which can further explain the even higher ~1 at.% density of retained hydrogen in the
16 first ~0.1 μm below the surface of plasma exposed tungsten. It is plausible that for such high
17 hydrogen concentrations and low temperatures, when almost all hydrogen is trapped, the platelets
18 may serve as seeds for formation of cracks and blisters, which are often observed under such
19 conditions on plasma-exposed tungsten surfaces and resemble geometry of the platelets [6].

20 The performed analysis of dynamics of the hydrogen trapped by the platelets under outgassing
21 conditions shows that the platelets gradually decay on time scale from days to several months at
22 the room temperature, which is consistent with the experimentally observed decrease of the
23 amount of retained hydrogen in the tungsten samples for extended storage times. It is also shown
24 that for typical dislocation densities in ITER grade tungsten samples, the formation of the platelets
25 can effectively slow hydrogen diffusion in tungsten. However, this effect is not significant at the
26 temperatures ~600 K and higher.

27 Therefore, the described properties of the self-trapped hydrogen structures and the developed
28 model allow to resolve difficulties in explaining experimental findings on retention of large
29 quantities of hydrogen in tungsten. We should note that the proposed earlier hydrogen retention
30 mechanism due to creation of super abundant vacancies [33] presumes existence of extremely high
31 interstitial hydrogen concentrations ~50 at.%, which is much higher than simulated in this work.
32 Nevertheless, the simulated nature of the platelet-like structures and the corresponding model
33 extrapolations need further experimental validation. In particular, the induction of the hydrogen
34 platelet formation by non-hydrostatic tensile or shear stresses could be experimentally verified in
35 a straightforward way. Furthermore, the details of hydrogen transport in vicinity of the platelets in
36 tungsten are not yet clear, as the generated stresses can induce hydrogen drifts not considered in
37 the presented model. The possibility of formation of dislocations facilitated by hydrogen and
38 neutron irradiation and its impact on hydrogen retention also require further studies.

51 52 53 **Acknowledgements**

54 This material is based upon the work supported by the U.S. Department of Energy, Office of
55 Science, Office of Fusion Energy Sciences under Award No. DOE DE-SC0018302 at UCSD.
56
57

References

- [1] G. Federici, C. H. Skinner, J. N. Brooks, J. P. Coad, C. Grisolia, A. A. Haasz, A. Hassanein, V. Philipps, C. S. Pitcher, and J. Roth, *Nucl. Fusion* **41** (2001) 1967.
- [2] J. Roth, E. Tsitrone, A. Loarte, Th. Loarer, G. Counsell, R. Neu, V. Philipps, S. Brezinsek, M. Lehnen, P. Coad, Ch. Grisolia, K. Schmid, K. Krieger, A. Kallenbach, B. Lipschultz, R. Doerner, R. Causey, V. Alimov, W. Shu, O. Ogorodnikova, A. Kirschner, G. Federici, and A. Kukushkin, *J. Nucl. Mater.* **390–391** (2009) 1.
- [3] R. A. Pitts, S. Carpentier, F. Escourbiac, T. Hirai, V. Komarov, A. S. Kukushkin, S. Ligo, A. Loarte, M. Merola, and R. Mitteau, *J. Nucl. Materials* **415** (2011) S957.
- [4] “ITER Plant Description Document”, G A0 FDR 1 01-07-13 R1.0, Chap. 5, p. 13.
- [5] G. Federici and C. H. Skinner, “Tritium inventory in the materials of the ITER plasma-facing components”, in *Nuclear Fusion Research* (Springer, 2005), pp. 287-317.
- [6] T. Tanabe, *Phys. Scr.* **T159** (2014) 014044.
- [7] V. Kh. Alimov, W. M. Shu, J. Roth, K. Sugiyama, S. Lindig, M. Balden, K. Isobe, and T. Yamanishi, *Phys. Scr.* **T138** (2009) 014048.
- [8] O. V. Ogorodnikova, *J. Appl. Phys.* **118** (2015) 074902.
- [9] B. J. Merrill, M. Shimada, and P. W. Humrickhouse, *J. Plasma Fusion Res. SERIES 10* (2013) 71.
- [10] M. Poon, A. A. Haasz, and J. W. Davis, *J. Nucl. Materials* **374** (2008) 390.
- [11] E. A. Hodille, F. Ghiorghiu, Y. Addab, A. Založnik, M. Minissale, Z. Piazza, C. Martin, T. Angot, L. Gallais, M.-F. Barthe, C. S. Becquart, S. Markelj, J. Mougnot, C. Grisolia, and R. Bisson, *Nucl. Fusion* **57** (2017) 076019.
- [12] D. Terentyev, V. Dubinko, A. Bakaeva, Y. Zayachuk, W. Van Renterghem, and P. Grigorev, *Nucl. Fusion* **54** (2014) 042004.
- [13] D. F. Johnson and E. A. Carter, *J. Mater. Res.* **25** (2010) 315.
- [14] L. Sun, S. Jin, X.-C. Li, Y. Zhang, and G.-H. Lu, *J. Nucl. Materials* **434** (2013) 395.
- [15] N. Fernandez, Y. Ferro, and D. Kato, *Acta Materialia* **94** (2015) 307.
- [16] S. Plimpton, *J. Comp. Phys.* **117** (1995) 1.
- [17] L.-F. Wang, X. Shu, G.-H. Lu, and F. Gao, *J. Phys.: Condens. Matter* **29** (2017) 435401.
- [18] P. Zaleski-Ejgierd, V. Labet, T. A. Strobel, R. Hoffmann, and N. W. Ashcroft, *J. Phys.: Condens. Matter* **24** (2012) 155701.
- [19] T. Scheler, F. Peng, C. L. Guillaume, R. T. Howie, Y. Ma, and E. Gregoryanz, *Phys. Rev. B.* **87** (2013) 184117.
- [20] P. Hirel, *Comput. Phys. Comm.* **197** (2015) 212.
- [21] A. H. Cottrell and B. A. Bilby, *Proc. Phys. Soc. A* **62** (1949) 49.
- [22] R. D. Smirnov and S. I. Krasheninnikov, *Nucl. Fusion* **53** (2013) 082002.
- [23] H. B. Zhou, S. Jin, Y. Zhang, G. H. Lu, and F. Liu, *Phys. Rev. Lett.* **109** (2012) 135502.
- [24] K. Schmid, U. von Toussaint, and T. Schwarz-Selinger, *J. Appl. Phys.* **116** (2014) 134901.
- [25] J. Guterl, R. D. Smirnov, S. I. Krasheninnikov, M. Zibrov, and A. A. Pisarev, *Nucl. Fusion* **55** (2015) 093017.

- 1
2
3 [26] D. Terentyev, A. Dubinko, A. Bakaeva, G. De Temmerman, Fusion Eng. Des. **124** (2017)
4 405.
5
6 [27] W. R. Wampler and R. P. Doerner, Phys. Scr. **T138** (2009) 014037.
7 [28] R. C. Rau, Philosophical Magazine **18** (1968) 1079.
8 [29] J. Grzonka, Ł. Ciupiński, J. Smalc-Koziorowska, O. V. Ogorodnikova, M. Mayer, K. J.
9 Kurzydłowski, Nuclear Instruments and Methods in Physics Research B **340** (2014) 27.
10 [30] T. Koyanagi, N. A. P. Kiran Kumar, T. Hwang, L. M. Garrison, X. Hu, L. L. Snead, and Y.
11 Katoh, J. Nucl. Materials **490** (2017) 66.
12 [31] K. A. Moshkunov, K. Schmid, M. Mayer, V. A. Kurnaev, Yu. M. Gasparyan, J. Nucl.
13 Materials **404** (2010) 174.
14 [32] R. Bisson, S. Markelj, O. Mourey, F. Ghiorghiu, K. Achkasov, J.-M. Layet, P. Roubin, G.
15 Cartry, C. Grisolia, and T. Angot, J. Nucl. Materials **467** (2015) 432.
16 [33] Y. Fukai, Journal of Alloys and Compounds **256-257** (2003) 263.
17
18
19
20
21
22
23
24
25
26
27
28
29
30
31
32
33
34
35
36
37
38
39
40
41
42
43
44
45
46
47
48
49
50
51
52
53
54
55
56
57
58
59
60